Site Selectivity in Electrophilic (H^+, CH_3^+) Abstraction on $Os(H)_2X_2(P^iPr_3)_2$

Roger Kuhlman, William E. Streib, John C. Huffman, and Kenneth G. Caulton*

Contribution from the Department of Chemistry and Molecular Structure Center, Indiana University, Bloomington, Indiana 47405-4001

Received February 5, 1996[⊗]

Abstract: While protonation (HBF_4 or HO_3SCF_3 = HOTf) or methylation (MeOTf) of $Os(H)_2X_2L_2$ (L = P^iPr_3, X = Cl, Br) abstracts halide and causes aggregation to form $(L_2OsH_2)_2(\mu\text{-}X)_3^+$, protonation of $Os(H)_2I_2L_2$ forms a species whose −7.5 ppm ^{1}H NMR chemical shift has a short T_{1min} characteristic of an H_2 complex (or short H/H contact). This is also supported by a significant isotopic perturbation of resonance for $OsH_3I_2L_2^+$, although no J(HD) is observed in $OsHD_2I_2L_2^+$. In contrast, $Os(H)_2I_2L_2$ is converted by MeOTf into $L_2Os(H)_2(OTf)I$, then $L_2Os(H)_2(OTf)_2$, a non-octahedral Lewis acid which binds H_2O to form the intramolecularly hydrogen bonded $L_2Os(H)_2(OTf)_2(H_2O)$, whose intramolecular fluxionality has been characterized (^{1}H and ^{31}P NMR). The complexes $L_2Os(H)_2(OR_f)_2$ (OR_f = OCH_2CF_3 and $OCH(CF_3)_2$) are synthesized from $L_2Os(H)_2Cl_2$ and $TlOR_f$. The X-ray structure of $L_2Os(H)_2(OCH_2CF_3)_2$ shows evidence for O→Os π-donation. Protonation of $L_2Os(H)_2(OR_f)_2$ (R_f = $CH(CF_3)_2$) with HBF_4 forms $(L_2OsH_2)_2(\mu\text{-}F)_3^+$, which is also inefficiently formed by fluoride abstraction (25 °C) by $L_2Os(H)_2(OCH_2CF_3)_2$, even in the solid state. Protonation of the monochloride $L_2Os(H)_3Cl$ gives equimolar $(L_2OsH_2)_2(\mu\text{-}Cl)_3^+$ and $L_2OsH_7^+$, but the *initial* site of protonation remains unknown. Crystal data for $[OsH_2(P^iPr_3)_2(OTf)_2][OsH_2(P^iPr_3)_2(OTf)_2(H_2O)]$ at −172 °C: a = 19.916(3) Å, b = 20.260(4), c = 19.824(3), α = 115.54(1)°, β = 115.03(1), γ = 63.57(1) with Z = 4 in space group $P\bar{1}$. Crystal data for $(P^iPr_3)_2OsH_2(OCH_2CF_3)_2$ at −175 °C: a = 8.831(2), b = 16.680(4), c = 19.820(5), β = 93.97(1)° with Z = 4 in space group $P2_1/c$.

Introduction

A recent review[1a] of electrophilic (e.g., E = H^+, R^+, SiR_3^+) attack on transition metal hydrido halide (or pseudohalide) molecules has described the variety of possible outcomes: attack at metal, at hydride, or at halide. This can be followed by intramolecular (proton) migration or loss of H_2 or of HX. An informative new development[1b] in this field is the study of hydrogen bonding to hydrido/halide molecules, since this probes weak interactions which precede full proton transfer and can establish the selectivity for hydride vs halide as the more Brønsted basic site.

General rules and predictive capability remain elusive, however. One might generalize that protonation occurs at hydride ligands in preference to halide ligands, but this relies on a base of experience heavily skewed toward saturated, octahedral, and d^6 molecules. In sharp contrast, *no non-octahedral complex has ever been protonated at hydride in preference to halide.* The only halide-containing complexes of H_2 attached to non-octahedral metal centers are $(PR_3)_2RuXH(H_2)$, $(PR_3)_2OsX_2(H)_2(H_2)$,[2] and $(PR_3)_2OsX(H)_3(H_2)$, none of which are synthesized by protonation. Even in octahedral complexes, facile HCl loss and studies of hydrogen bonding have shown that the halide−dihydrogen vs hydride−hydrochloric acid equilibrium can be nearly thermoneutral. Both d^8 square planar[3a] $(PR_3)_2PtClH$ and d^4 trigonal antiprismatic $(PR_3)_2OsCl_2(H)_2$[4] are protonated at halide. Both of these complexes are formally unsaturated, which may be a determining characteristic. Furthermore, the d^2 eight-coordinate $(PR_3)_4WCl_2(H)_2$[3b] may very well initially interact with the incoming proton via its halide ligands. Thus, a greater number of *structure types* have shown preference for protonation at halide. The total number of examples remains low, but this may be due primarily to the relative dearth of studies on alternate structure types. Moreover, in protonolysis reactions, steric factors must be considered when there is direct competition of different sites within a molecule for an electrophile. The possibilities of hydrogen bonding to coordinated halide ligands should be recognized in $MX(H_2)$ complexes, even though such interactions are not as easily detected as H−H bonding. Hydrogen bonding to metal-bound hydride or halide can be an important structural influence.

As a final point of introduction to this report, we note that *unsaturated* (16-electron) complexes containing a dihydrogen ligand are very rare. The only examples currently known are a d^8 4-coordinate Pt complex[5] and a d^6 five-coordinate Ru complex.[6] This class of compounds has almost certainly been neglected because of the difficulty of synthesis. While protonation of unsaturated metal hydrides is a potentially viable technique, it can be complicated by the attendant ligands frequently encountered in unsaturated complexes. That is, a lone pair on the α-atom of a pseudohalide ligand provides an alternate site for protonation. We have recently *attempted* the synthesis of a d^4 six-coordinate dihydrogen complex, $L_2OsH(H_2)Cl_2^+$ (L = P^iPr_3), by protonation of $L_2OsH_2Cl_2$ (**1**). However, we found[4] a product derived from protonation at chloride, not hydride: $[L_2OsH_2]_2(\mu\text{-}Cl)_3^+$ (**4**). Peris and co-

[⊗] Abstract published in *Advance ACS Abstracts,* July 1, 1996.

(1) (a) Kuhlman, R. Submitted for publication. (b) Crabtree, R. H.; Siegbahn, P. E. M.; Eisenstein, O.; Rheingold, A. L.; Koetzle, T. F. *Acc. Chem. Res.* In press.

(2) Assuming only one H_2 ligand in these complexes. These complexes lose HX under phase-transfer (toluene/water) conditions and H_2 atmosphere.

(3) (a) Kuhlman, R.; Rothfuss, H.; Gusev, D. G.; Streib, W. E.; Caulton, K. G. *Abstracts of Papers*; 209th National Meeting of the American Chemical Society; American Chemical Society: Washington, DC, 1995; *INOR* 497. (b) Rothfuss, H.; Gusev, D. G.; Caulton, K. G. *Inorg. Chem.* **1995**, *34*, 2894.

(4) Kuhlman, R.; Streib, W. E.; Caulton, K. G. *Inorg. Chem.* **1995**, *34*, 1788.

(5) Gusev, D. G.; Notheis, J. U.; Rambo, J. R.; Hauger, B. E.; Eisenstein, O.; Caulton, K. G. *J. Am. Chem. Soc.* **1994**, *116*, 7409.

(6) Chaudret, B.; Chung, G.; Eisenstein, O.; Jackson, S. A.; Lahoz, F. J.; Lopez, J. A. *J. Am. Chem. Soc.* **1991**, *113*, 2314.

S0002-7863(96)00369-1 CCC: $12.00

workers have demonstrated that hydrogen-bond strength to metal-bound halides follows the order Cl > Br > I, and also that hydrogen bonding to a hydride ligand is quite sensitive to the other ligands on the metal.[7] Since formation of a hydrogen bond is an initial step in proton-transfer reactions, we anticipated possibly different reactivity for the heavier halide analogs of $L_2OsH_2Cl_2$. We therefore decided to further investigate electrophilic additions to complexes $L_2OsH_2X_2$ (X = Cl, Br, I). These complexes offer an opportunity to investigate the direct competition of halide and hydride for a proton, since unsaturated complexes (Lewis acids) should be less likely to be protonated at the metal center itself. We also anticipated that protonolysis of a ligand in a complex which is already unsaturated could lead to interesting subsequent reactivity.

Results

Electrophilic Additions to $L_2OsH_2X_2$ (L = P^iPr_3; X = Cl, Br, I). (a) Formation of $[[L_2OsH_2]_2(\mu\text{-}X)_3]^+$ (X = Cl (4), Br (5)). The dichloride complex $L_2OsH_2Cl_2$ (**1**) reacts with strong

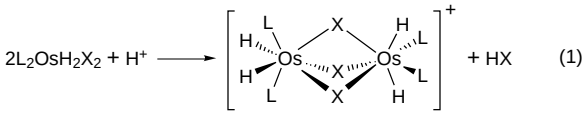

(1)

acids (HBF_4, HOTf) to form a trihalide bridged species, **4** (eq 1). The same product is observed with other electrophiles: MeOTf, Me_3SiOTf, and AgOTf. However, reaction with $AgBF_4$ does *not* yield **4**, but rather gives a mixture of two new hydride-containing complexes (*vide infra*).

The dibromide complex $L_2OsH_2Br_2$ (**2**) reacts with HBF_4 or HOTf to lose HBr and form a tribromide-bridged diosmium species, in a manner wholly analogous to eq 1. The same product, $[\{L_2OsH_2\}_2(\mu\text{-}Br)_3]^+$ (**5**), is formed by addition of MeOTf or Me_3SiOTf, with release of 0.5 equiv of MeBr or Me_3SiBr, respectively. The tribromide-bridged species (**5**) is easily identified by ^1H and ^{31}P NMR, IR, and elemental analysis. The only difference between the protonation reactions of **1** and **2** is that the dibromide reacts more slowly. For example, protonation (HBF_4) of **2** in dichloromethane requires about 4 h at room temperature to go to completion, whereas the reaction with **1** is complete in 15 min in the same solvent.

(b) Reactions of $[L_2OsH_2]_2(\mu\text{-}Cl)_3^+$ (4). Although these trihalide bridged species contain formally 18-electron metal centers, they react with nucleophiles, presumably by first breaking a halide bridge. It has been mentioned[4] that Cl^- (in the form of $Bu_4N^+Cl^-$) splits **4** (eq 2) to re-form the original starting material (**1**).

$$[\{L_2OsH_2\}_2(\mu\text{-}Cl)_3]^+ + Cl^- \rightarrow 2L_2OsH_2Cl_2 \qquad (2)$$

One equivalent of **4** reacts with *five* equivalents of CO to form two octahedral products, $L_2OsCl_2(CO)_2$ (**6**) and $L_2OsCl(CO)_3^+$ (**7**) (eq 3). Accordingly, two ^{31}P signals are observed, and no hydride signals in ^1H NMR. Pseudoquartets in the

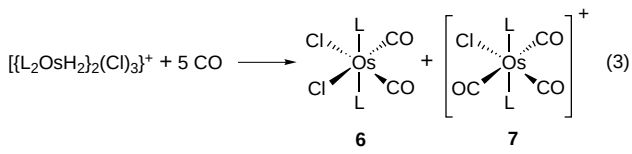

(3)

methyl region indicate that the two complexes each have trans phosphines. These complexes are identified primarily from ^{13}C NMR of the ^{13}CO-labeled complexes. Three ^{13}C signals in a 2:2:1 ratio are seen when ^{13}CO is added to **4**. All signals show coupling to ^{31}P (J_{CP} = 6−8 Hz). The resonance at 176.9 ppm has no additional coupling, and is assigned to **6**. The spectroscopic signature of **6** was confirmed by independent preparation from ^{13}CO and **1**. Based on the observation of two CO stretching frequencies,[8] this complex is assigned to have cis chlorides and cis carbonyls. The two remaining ^{13}C resonances (of **7**) are mutually coupled. The signal at 168.6 ppm is coupled to two ^{13}C (1C, J_{CC} = 3.9 Hz), while that at 176.6 ppm is coupled to one ^{13}C (2C, J_{CC} = 3.9 Hz). These signals are assigned to the CO trans to Cl and the two CO's cis to Cl in **7**, respectively. Equation 3 thus represents a μ_2-halide bridge-splitting reaction, with the *two* monomeric products determined by retention of only three chlorides.

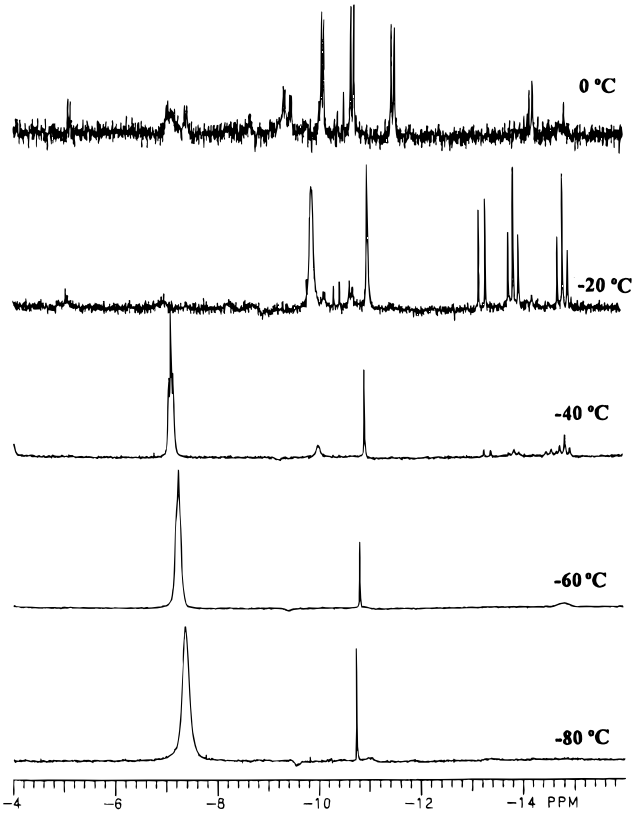

Figure 1. Variable-temperature ^1H NMR (hydride region, CD_2Cl_2) of $[L_2OsH(H_2)I_2]^+$. The evolution of spectra (from bottom to top) demonstrate the irreversible decomposition of this complex.

Protonation of $(P^iPr_3)_2OsH_2I_2$. Unlike **1** or **2**, $L_2OsH_2I_2$ (**3**) does not react with electrophiles to give trihalide-bridged products. Instead, $L_2OsH_2I_2$ is protonated at low temperature (<−40 °C) to form primarily one product (**8**), which reacts further at high temperatures, giving LH^+ and unknown metal-containing products. Due to the metastability of **8**, complete characterization (elemental analysis, X-ray diffraction) is not feasible. However, by carefully preparing NMR samples below −40 °C, enough information can be obtained to draw some structural conclusions.

Figure 1 shows variable-temperature ^1H NMR taken from a sample of **8** prepared at low temperature and placed in a pre-cooled NMR probe at −70 °C. Thus, the evolution of the spectra (from bottom to top) is *irreversible*, and demonstrates both the characterization and the decomposition of **8**. The experiment has been repeated several times, and formation of **8** is quite reproducible. The initial conversion is almost exclusively to **8** (−7.5 ppm), with a slight impurity at −10.7 ppm. Correspondingly, one sharp ^{31}P resonance is observed at

(7) Peris, E.; Lee, J. C., Jr.; Rambo, J. R.; Eisenstein, O.; Crabtree, R. H. *J. Am. Chem. Soc.* **1995**, *117*, 3485.

(8) Kent Renkema, personal communication.

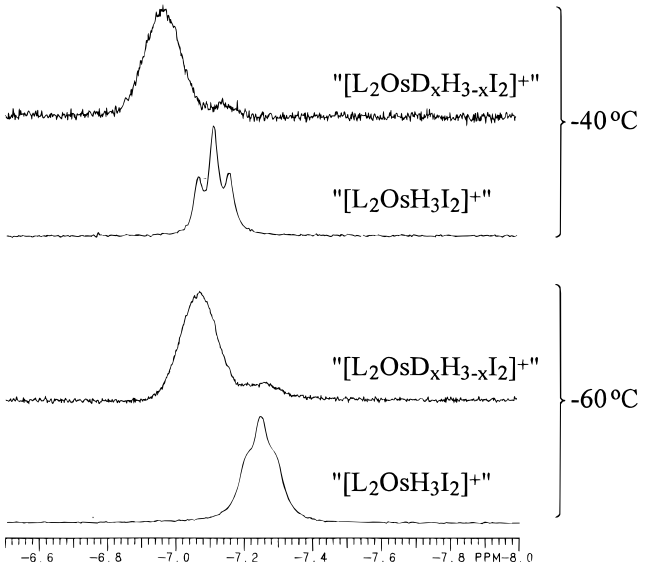

Figure 2. Hydride region of ^{1}H NMR of $[L_2OsH_xD_{3-x}I_2]^+$ and $[L_2OsH_3I_2]^+$ in CD_2Cl_2, showing isotopic perturbation of resonance.

99.4 ppm, with a much smaller (<5%) signal at 53.8 ppm. Unlike the spectra of **4**, which have several resonances at low temperature due to slowed rotation about Os−P bonds,[4] the hydride signal of **8** does not decoalesce even at −90 °C. Similarly, the ^{31}P resonance at −70 °C is a sharp singlet (line width = 20 Hz), and not significantly broader at −80 °C. Thus, the assignment of **8** as $[\{L_2OsH_2\}_2(\mu\text{-}I)_3]^+$ seems unreasonable. Attempts to obtain a selectively hydride-coupled ^{31}P spectrum were unsuccessful.

Fortunately, the minimum T_1 value for the hydride signal of **8** occurs within the temperature regime of the stability of this complex (−77 °C, 32 ms, 300 MHz). The hydrides in **8** are relaxing much faster than those in **1** or **4** ($T_{1\text{min}} \sim 200$ ms), indicating some close H−H contact(s) in this product. In order to gain more information, partially deuterated (∼70% D) **3** was protonated with DOTf to form d_x-**8**. ^{1}H NMR spectra of **8** and d_x-**8** are shown at two temperatures in Figure 2. These spectra were recorded sequentially and on the same instrument, so the temperatures of the two spectra are identical. No HD coupling is observed; in fact, the resonance of d_x-**8** is not even significantly broadened (for example, the hydride signal of d_x-**8** is 3 Hz broader than that of **8** at −60 °C). Most remarkable is the 180 ppb *downfield* shift of the resonance upon deuteration. The usual (intrinsic) isotopic shift is much smaller and upfield.[9] This unusual ipr (isotopic perturbation of resonance) indicates that the observed resonance is averaged over different sites, one or more of which deuterium thermodynamically prefers over the other(s). Such ipr is commonly observed for complexes containing an agostic interaction,[10] or dihydrogen ligand. This behavior of **8** is remarkably similar to that observed by Heinekey and Oldham in d_x-$(Tp)Ir(PMe_3)H(H_2)^+$.[11] Assuming the formula $L_2OsHI_2(H_2)^+$, an H−H distance of 1.22 Å is calculated in the H_2 ligand,[12] which is considered a "stretched" dihydrogen ligand.

One additional important observation is that the hydride chemical shift is quite temperature dependent, moving from −7.45 ppm at −88 °C to −7.04 ppm at −28 °C. This temperature dependence might suggest a temperature-dependent equilibrium. One possible interpretation is an equilibrium mixture of $L_2OsHI_2(H_2)^+$ and $L_2Os(H)_3I_2^+$. We also recognize the possibility of hydrogen bonding between a hydride and an iodide ligand, or even a complex of HI as a participant in the equilibrium. In fact, by comparison with protonation reactions of **1** and **2**, which eliminate HX, it seems plausible that there might be some type of H−I bonding in **8**. Thus, we consider an alternate equilibrium (eq 4), involving an H_2 complex and an HI complex. In either case, the most prevalent structure is most likely $[L_2OsHI_2(H_2)]^+$.

$$[L_2OsHI_2(H_2)]^+ \rightleftharpoons [L_2Os(H)_2I(HI)]^+ \qquad (4)$$

This remarkable difference in reactivity of iodide from the other halides can be rationalized from background experimental results. As mentioned earlier, the gas-phase basicity of iodide is the lowest of the halides, and this trend seems also to hold true for coordinated iodide in this case. Furthermore, the hydride ligands in **3** are likely to be more basic than those in **1** and **2**, due to the better $\sigma + \pi$ donor power of iodide to a metal. These two factors may alter the relative *thermodynamics* of protonation of halide vs hydride. With the hydride ligands nearly "buried" in the phosphine ligands, iodide still seems to be the most accessible proton acceptor. Even if iodide is the kinetic site of protonation, it is not surprising that the HI complex intermediate is long-lived enough to effect intramolecular proton transfer prior to any intermolecular reactions (as observed for the lighter halides).

By −20 °C, **8** is consumed, and at least five new hydride signals appear. One interesting point is that one of the hydride signals is a doublet, indicating coupling to only one phosphorus. Since one final protonation product is LH^+, phosphine loss is to be expected in intermediate reaction steps. More hydride doublets appear at 0 °C, indicating further phosphine loss. After 1 h at 20 °C, the hydride region of the spectrum (not shown) is devoid of signals. The only final product observed by ^{1}H and ^{31}P NMR is $P^iPr_3H^+$.

When **3** is reacted with excess DOTf in CH_2Cl_2, the phosphonium product is almost exactly $^1/_3$ deuterated—the LH^+/LD^+ ratio is 2:1, determined by ^{31}P NMR integration of the well-resolved signals. This ratio is unchanged after 2 h at room temperature, indicating no exchange with the acid. Thus, it seems likely that proton transfer to the phosphine occurs intramolecularly (as opposed to phosphine dissociation and subsequent protonation). Deuterium NMR shows signals for DOTf (at 11.3 ppm), and LD^+ (at 5.30 ppm, doublet), and two unassigned resonances at 2.94 and 7.41 ppm.

Reaction of $(P^iPr_3)_2OsH_2I_2$ (3) with MeOTf. The reaction of the diiodide complex with MeOTf is also different than that for the lighter halide complexes. Methyl triflate (2 equiv) reacts with **3** over a period of 12 h in CD_2Cl_2 at room temperature, to eventually yield a single product, **9**. This product is characterized by a single ^{31}P NMR signal, a doublet of doublets in the methyl region, and a triplet in the hydride region of ^{1}H NMR. These signals are characteristic of the L_2OsH_2 substructure found in complexes **1**−**5**. We investigated the structure of **9** by single crystal X-ray diffraction. A solution of **9** in CH_2Cl_2 was layered with ether. The crystals grew over a period of 10 days, and are actually 1:1 cocrystals of $L_2OsH_2(OTf)_2$ (**9**) and $L_2OsH_2(OTf)_2(H_2O)$ (**10**). Presumably, H_2O from the air entered the flask during the crystallization process. Although **9** and **10** reside in the same unit cell, they are independent molecules with no significant intermolecular interactions. Therefore, the structures of the two molecules are discussed separately. Furthermore, the unit cell contains two crystallographically-independent molecules each of **9** and **10**. Values for each are given; there are no significant deviations between the two molecules for either complex. All hydride ligands were placed

(9) Luo, X. L.; Crabtree, R. H. *J. Am. Chem. Soc.* **1990**, *112*, 4813.
(10) Calvert, R. B.; Shapley, J. R. *J. Am. Chem. Soc.* **1978**, *100*, 7726.
(11) Heinekey, D. M.; Oldham, W. J., Jr. *J. Am. Chem. Soc.* **1994**, *116*, 3137.
(12) $R^* = 5.0$ s^{-1} from $T_{1\text{min}}$ of **1**, **2**, or **3**. $R_{HH} = {}^3/_2\,(1/T_{1\text{min}} - R^*)$.

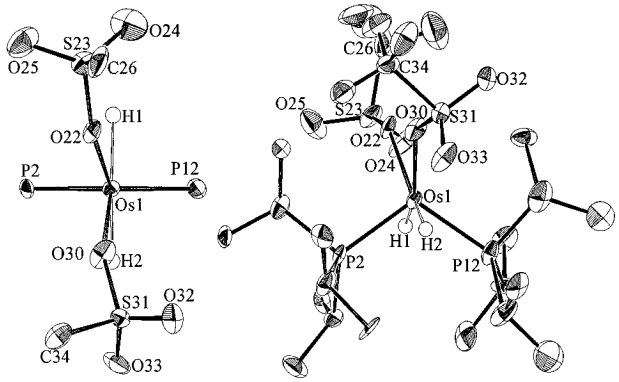

Figure 3. Two ORTEP views of $L_2OsH_2(OTf)_2$ (molecule A).

Table 1. Bond Distances and Angles for $L_2OsH_2(OTf)_2$[a]

	distance(Å)	
	A	B
Os(1)−P(2)	2.265(5)	2.268(5)
Os(1)−P(12)	2.267(5)	2.269(5)
Os(1)−O(22)	2.13(1)	2.13(1)
Os(1)−O(30)	2.15(1)	2.13(1)
	angle (deg)	
	A	B
P(2)−Os(1)−P(12)	112.8(2)	112.8(2)
P(2)−Os(1)−O(22)	106.3(4)	107.8(3)
P(2)−Os(1)−O(30)	110.8(4)	116.0(4)
P(12)−Os(1)−O(22)	127.4(4)	125.3(3)
P(12)−Os(1)−O(30)	119.5(4)	115.3(4)
O(22)−Os(1)−O(30)	74.3(5)	74.8(5)
Os(1)−O(22)−S(23)	135.7(8)	133.0(7)
Os(1)−O(30)−S(31)	140.2(9)	139.5(8)

[a] Values are given for each of the two independent molecules (A and B).

in idealized positions using the program XHYDEX, which found no positions of reasonable energy other than those shown.

Structure of $L_2OsH_2(O_3SCF_3)_2$ (9). An ORTEP representation of **9** is shown in Figure 3, and selected bond distances and angles are given in Table 1. The structure of this complex is similar to those of **1**[13] and of $L_2OsH_2(OCH_2CF_3)_2$. The coordination geometry of **1** has been described as a 4:2 structure,[14a] where *4* refers to the two P and two H ligands in one molecular hemisphere, and *2* to the two Cl ligands in the other hemisphere. The non-octahedral character of these structures has been discussed in detail,[14a] and can also be traced to the Jahn−Teller effect.[14b] Complex **9** also falls into this category. The *4* substructure (OsP_2H_2) of **9** is nearly identical to that of **1**. The P3−Os−P13 angle is 112.8(2)°, and the HOsH plane is perpendicular to POsP. However, as one would predict for the bulkier and weaker-donating $CF_3SO_3^-$ ligands, the *2* substructure is rotated so that the O−Os−O plane is almost coplanar with the H−Os−H plane. The structure of **9** is best described as 4:2 with $\omega = 85°$ (the intersection angle of the O22−Os−O30 and P2−Os−P12 planes). This arrangement is the worst in terms of σ-bonding (but the weak triflate ligands are apparently able to be *trans* to hydrides), but also minimizes the unfavorable triflate−phosphine steric interactions (definitely more important for triflate than chloride). The O22−Os−O30 angle is quite acute (74.3(5)°), a characteristic observed in other ditriflate metal complexes.[15] The Os−O22 and Os−O30 distances (2.13(1) and 2.15(1) Å) are similar to metal-oxygen distances in other 5d metal triflate complexes.[15]

Structure of $L_2OsH_2(O_3SCF_3)_2(H_2O)$ (10). This seven-coordinate complex is simply a water adduct of **9**. It thus

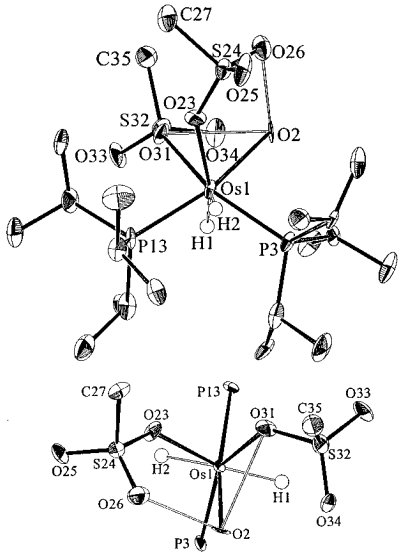

Figure 4. Two ORTEP representations of $L_2OsH_2(OTf)_2(H_2O)$ (molecule A). The bottom figure emphasizes the proposed hydrogen bonding (open bars between O's indicate probable locations of hydrogen bonds).

Table 2. Selected Bond Distances and Angles for $L_2OsH_2(OTf)_2(H_2O)$[a]

	distance (Å)	
	A	B
Os(1)−P(3)	2.305(5)	2.307(5)
Os(1)−P(13)	2.325(5)	2.327(5)
Os(1)−O(2)	2.219(12)	2.219(12)
Os(1)−O(23)	2.270(11)	2.189(13)
Os(1)−O(31)	2.176(11)	2.266(13)
	angle (deg)	
	A	B
P(3)−Os(1)−P(13)	112.5(2)	112.2(2)
P(3)−Os(1)−O(2)	80.5(3)	81.2(3)
P(3)−Os(1)−O(23)	118.8(3)	147.3(4)
P(3)−Os(1)−O(31)	148.5(4)	118.9(3)
P(13)−Os(1)−O(2)	165.6(3)	165.5(3)
P(13)−Os(1)−O(23)	95.7(3)	90.1(4)
P(13)−Os(1)−O(31)	89.8(4)	96.7(4)
O(2)−Os(1)−O(23)	82.4(5)	75.4(5)
O(2)−Os(1)−O(31)	75.8(4)	80.6(5)
O(23)−Os(1)−O(31)	78.4(5)	79.6(5)
Os(1)−O(23)−S(24)	138.1(8)	130.2(8)
Os(1)−O(31)−S(32)	128.6(7)	139.4(8)

[a] There are two independent molecules (A and B) in the unit cell.

"proves" the unsaturation of **9** itself. Two ORTEP drawings of **10** are shown in Figure 4; Table 2 displays selected bond distances and angles. Although the hydrogens on O2 were not located in the diffraction data, assignment of the ligand as water is supported by a long Os−O2 distance[16] (2.22(1) Å). Osmium oxo bond lengths are generally about 1.74 Å,[17] while those of

(13) Aracama, M.; Esteruelas, M. A.; Lahoz, J. A.; Meyer, U.; Oro, L. A.; Werner, H. *Inorg. Chem.* **1991**, *30*, 288.

(14) (a) Gusev, D. G.; Kuhlman, R.; Rambo, J. R.; Berke, H.; Eisenstein, O.; Caulton, K. G. *J. Am. Chem. Soc.* **1995**, *117*, 281. (b) Kubáček, P.; Hoffmann, R. *J. Am. Chem. Soc.* **1981**, *103*, 4320.

(15) (a) Danopoulos, A. A.; Wilkinson, G.; Hursthouse, M. B.; Hussain, B. *Polyhedron* **1989**, *8*, 2947. (b) Chisholm, M. H.; Kramer, K. S.; Martin, J. D.; Huffman, J. C.; Lobkovski, E. B.; Streib, W. E. *Inorg. Chem.* **1992**, *31*, 4469. (c) Harding, P. A.; Robinson, S. D.; Henrick, K. *J. Chem. Soc., Dalton Trans.* **1988**, 415. (d) Blosser, P. W.; Gallucci, J. C.; Wojcicki, A. *Inorg. Chem.* **1992**, *31*, 2377.

(16) Other $Os-OH_2$ complexes (with distances ranging from 2.05 to 2.25 Å): (a) Saito, M.; Uehiro, T.; Ebina, F.; Iwamoto, T.; Ouchi, A.; Yoshino, Y. *Chem. Lett.* **1979**, 997. (b) Pandey, K. K.; Roesky, H. W.; Noltemeyer, M.; Sheldrick, G. M. *Z. Naturforsch., Teil B* **1984**, *39*, 390. (c) Conway, C.; Kemmitt, R. D. W.; Platt, A. W. G.; Russell, D. R.; Sherry, L. J. S. *J. Organomet. Chem.* **1985**, *292*, 419. (d) Cotton, F. A.; Dunbar, K. R.; Matusz, M. *Inorg. Chem.* **1986**, *25*, 1589. (e) Edwards, C. F.; Griffith, W. P.; Williams, D. J. *J. Chem. Soc., Dalton Trans.* **1992**, 145.

osmium hydroxides are about 1.96 Å.[18] The short O2−O26 and O2−O31 of 2.682 and 2.708 Å, respectively, indicate intramolecular hydrogen bonding between the water and triflate oxygen atoms. Such O−O distances involving hydrogen bonding for similar complexes range from 2.65 to 2.95 Å.[19] The O26−O2−O31 angle of 91° is reasonable assuming non-linear hydrogen bonding. There are two other oxygen atoms within 3 Å of O2: O2−O34 (2.784 Å) and O2−O23 (2.943 Å). One hydride ligand (H1) lies approximately 2.83 Å from O2. These close contacts leave open the possibility of other hydrogen bonds, or bifurcated hydrogen bonds involving these other atoms. The nearest fluorine atom is 3.60 Å away from O2.

The OsP_2H_2 substructure is almost unchanged by the added H_2O ligand, maintaining a P3−Os−P13 angle of 112.5(2)° and a P−Os−P plane perpendicular to H−Os−H. The two triflate ligands accommodate the added ligand by leaning toward P13, as evidenced by the following P−O separations: O23−P13 = 3.41 Å, O31−P13 = 3.17 Å < O23−P3 = 3.93 Å, O31−P3 = 4.32 Å. See especially Figures 3 and 4. The O23−Os−O31 angle (78.4(5)°) is only slightly larger than it is in **10** (74.3-(5)°). The Os1−O23 bond length (2.27(1) Å) is significantly longer than Os1−O31 (2.18(1) Å), most likely because O23 is pseudo-trans to a hydride ligand. The H1−Os1−O23 angle is 158°, while H2−Os1−O31 is 139°. This difference in Os−O bond distances supports the XHYDEX placement of the hydride ligands.

Mechanism of Formation of $L_2OsH_2(OTf)_2$ (9). When this reaction is performed in an NMR tube, an intermediate (**11**) is observed with ^{1}H NMR spectroscopic features similar to those of **3** and **9** (see Experimental Section). Signals for this complex grow in and then disappear as the reaction proceeds. Also, a singlet at the chemical shift of MeI (2.16 ppm) increases in intensity as the reaction progresses. The most likely identity of this intermediate (**11**) is $L_2OsH_2I(OTf)$. When **3** and **9** are combined in CD_2Cl_2, a mixture of **3**, **9**, and **11** is observed by NMR after 15 min. at 20 °C. This experiment supports the assigned formula for **11**.[20] These observations indicate that the reaction proceeds as shown in eqs 5 and 6.

$$L_2OsH_2I_2 + MeOT_f \rightarrow L_2OsH_2I(OT_f) + MeI \quad (5)$$

$$L_2OsH_2I(OT_f) + MeOT_f \rightarrow L_2OsH_2(OTf)_2 + MeI \quad (6)$$

Spectroscopic Characterization and Reactions of $L_2OsH_2(OTf)_2$ (9) and $L_2OsH_2(OTf)_2(H_2O)$ (10). Complex **9** is a red-brown solid, soluble in dichloromethane and chloroform and slightly soluble in arenes. One reaction of **9** has already been mentioned—facile coordination of H_2O. In fact, reactivity studies of **9** are complicated by the frequent contamination of **9** with **10**. In this case, coordination of water is especially exergonic since *three* bonds are formed (Os−O and two hydrogen bonds). Similar behavior has been encountered by other researchers working with unsaturated metal triflate complexes.[21]

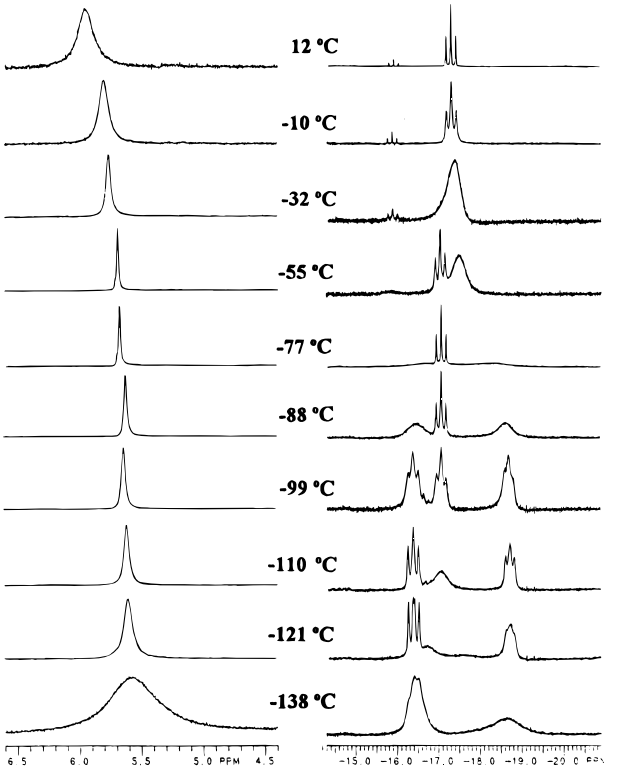

Figure 5. Variable-temperature ^{1}H NMR (hydride and water regions) of $L_2OsH_2(OTf)_2$ and $L_2OsH_2(OTf)_2(H_2O)$ in $CDFCl_2/CDF_2Cl$.

Variable-temperature ^{1}H NMR spectra of a mixture of **9** and **10** in freons are shown in Figure 5, where the ratio of H_2O to total Os is less than 1. At room temperature, only one hydride signal is observed in a mixture of **9** and **10**, indicating a fast exchange of water among osmium centers. The triplet structure of this signal indicates that neither the Os−H nor the Os−P bonds are broken in this dynamic process. As shown in Figure 5, the water resonance shows some temperature dependence, probably reflecting a temperature-dependent equilibrium binding of H_2O (averaged chemical shift of contributions from free and coordinated H_2O). Low-temperature broadening of this signal is consistent with hydrogen bonding. The hydride signal decoalesces into three resonances at −88 °C and below. The triplet at −17.1 is assigned to **9**, while the two other signals at −16.4 and −18.7 ppm are assigned to hydride resonances of **10**. Below −100 °C, the hydride resonance for **9** broadens and starts to decoalesce in a manner reminiscent of **1**−**3**. The signals overlap too much with those of **10** for a clear analysis.

At −121 °C, the signal at −16.4 ppm is clearly observed as a doublet of doublets with J = 33 and 43 Hz to two inequivalent ^{31}P nuclei, as would be expected from the structure in Figure 4. The other resonance is broader, so that the best resolution is of a triplet signal at −100 ppm, with J = 30 Hz. The broadness of this hydride signal at low temperature *may* be a result of hydride−ligand involvement in hydrogen bonding with coordinated water.

Decoalescence of the hydride signals in **10** indicates that hydride site-exchange is slowed, *and* that "spinning" of the $(OTf)_2(H_2O)$ moiety is slowed at this temperature. Thus, the coalescence process of **10** in the temperature range −99 to −55 °C could be hydride site-exchange, or rotation of the $(OTf)_2(H_2O)$ moiety. One other possible mechanism is triflate dissociation, and re-association.

In the presence of more H_2O (about 1.1 equiv), spectra of **10** alone can be analyzed. The ^{31}P NMR spectra of a sample of

(17) Galas, A. M. R.; Hursthouse, M. B.; Behrman, E. J.; Midden, W. R.; Green, G.; Griffith, W. P. *Transition Met. Chem.* **1981**, *6*, 194.

(18) Clark, G. R.; Waters, J. M.; Whittle, K. R. *J. Chem. Soc., Dalton Trans.* **1975**, 463.

(19) (a) 2.814, 2.953: Prins, R.; Birker, P. J. M. W. L.; Haasnoot, J. G.; Verschoor, G. C.; Reedijk, J. *Inorg. Chem.* **1985**, *24*, 4128. (b) 2.68, 2.65: Harding, P. A.; Robinson, S. D.; Henrick, K. *J. Chem. Soc., Dalton Trans.* **1988**, 415. (c) 2.83, 2.77, 2.75, 2.72, 2.82 Alilou, E. H.; Amadei, E.; Giorgi, M.; Réglier, M. *J. Chem. Soc., Dalton Trans.* **1993**, 549. (d) 2.81, 2.76, 2.76: Frank, W.; Reiss, G. J.; Schneider, J. *Angew. Chem., Int. Ed. Engl.* **1995**, *34*, 2416.

(20) Reaction of **1** with **2**, for example, yields a mixture of **1**, **2**, and L_2OsH_2ClBr. See ref 14.

(21) Komiya, S.; Huffman, J. C.; Kochi, J. K. *Inorg. Chem.* **1977**, *16*, 2138.

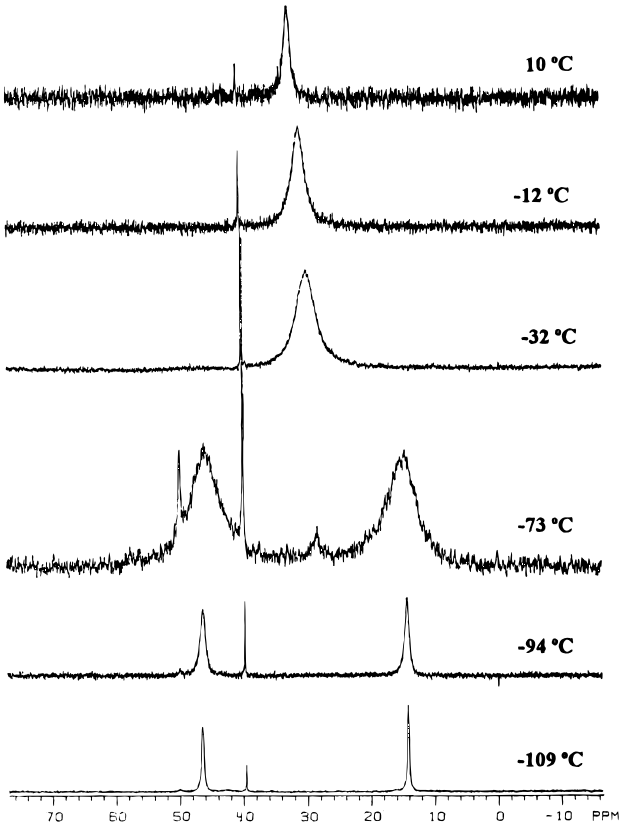

Figure 6. Variable-temperature ^{31}P NMR of $L_2OsH_2(OTf)_2(H_2O)$ in $CDFCl_2/CDF_2Cl$.

Table 3. Rate Constants for the Coalescence Process in $L_2OsH_2(OTf)_2(H_2O)$

^{31}P		^{1}H	
T	*k*	*T*	*k*
−94	280	−99	95
−73	2200	−83	490
−53	19000	−66	3000
−32	80000	−49	14500

10 are shown in Figure 6 (^1H NMR hydride signals are essentially the same as in the mixture, so they are not shown again). At +10 °C, the resonance represents coalesced signals of **9** and **10**, since there is still an equilibrium population of **9**. As the sample is cooled to −32 °C, water coordination is essentially quantitative and spectra are for **10** alone. Below this temperature, the resonance from **10** broadens and decoalesces. Rate constants (Table 3) for the exchange which causes this decoalescence were obtained by simulation of spectra using the program DNMR5. The decoalescence of the two hydride signals in this sample was also analyzed by simulations. As shown in Figure 7, the two plots are identical within experimental error, indicating that the same process is responsible for decoalescence of the hydrides and of the phosphorus nuclei. Eyring analysis of the data set including *k* values from both ^1H and ^{31}P coalescence gives the following activation parameters: $\Delta H^{\ddagger} = 7.7(4)$ kcal/mol, and $\Delta S^{\ddagger} = -4(2)$ cal/(mol K).[22] The entropy of activation is nearly zero, while the enthalpy of activation is substantial for a seven-coordinate complex, usually assumed to be highly fluxional. Triflate dissociation (as well as H_2O dissociation) can now be ruled out as the coalescence mechanism by the $\Delta S^{\ddagger}$ value, which suggests an intramolecular process. Hydride site exchange alone does not explain the

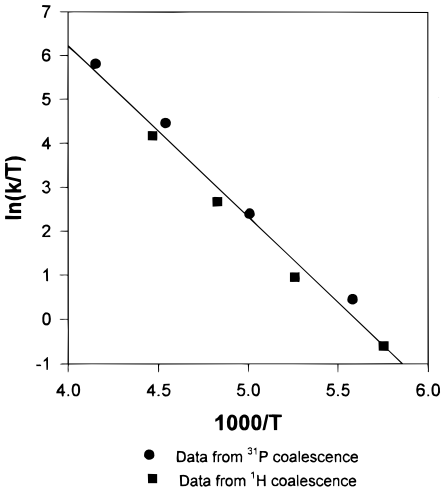

Figure 7. Eyring plot for decoalescence in $L_2OsH_2(OTf)_2(H_2O)$, observed by both ^{31}P and ^{1}H NMR.

Scheme 1

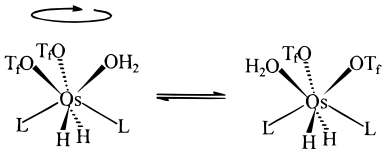

equivalence of rate for ^1H to ^{31}P coalescence. Therefore, the process almost certainly corresponds to rotation of the $(OTf)_2(H_2O)$ hemisphere of the complex with respect to the L_2H_2 hemisphere (Scheme 1).

If >1 equiv of water is added to a CD_2Cl_2 solution of **9**, additional reactions occur, as evidenced by a change in chemical shift of the hydride signal as more water is added. A hydride signal remains even after addition of about 40 equiv of H_2O. However, attempts to dissolve the complex in water led to decomposition. Water is most likely displacing triflate ligands, in a complex equilibrium involving species **9**, **10**, and one or more of the following: $L_2OsH_2(H_2O)_2(OTf)^+$, $L_2OsH_2(H_2O)_3^{2+}$, and $L_2OsH_2(H_2O)_2^{2+}$. Addition of excess MeCN gives the known dihydrogen complex, $L_2Os(MeCN)_3(H_2)^{2+}$.[26] Reaction of **9** with **1** effects partial conversion to **4**.

Summary of Electrophilic Reactions with 1−3. These reactions can be explained by electrophilic attack occurring initially at the halide ligand in all cases. The dichloride complex **1** reacts very quickly with electrophiles to form the trihalide-bridged product, **4**. The same reactions occur for the dibromide complex **2**, but more slowly. The diiodide complex reacts differently, and intermediates can be observed in the reactions. Protonation may begin at the halide (iodide) ligand, but the intermediate *observed* (**8**) is most likely a dihydrogen complex. For some reason (perhaps steric inhibition), $[L_2OsH_2]_2(\mu\text{-}I)_3^+$ is not formed; instead, the proton eventually migrates to the more basic ligand (P^iPr_3). Methylation of **3** occurs initially at iodide, perhaps forming a metastable cationic methyl iodide complex. Formation of a triiodide-bridged dimer does not occur, but the larger (than H^+) methyl group does not migrate to the

(22) Analyzing only data from ^{31}P coalescence gives $\Delta H^{\ddagger} = 7.6(3)$ kcal/mol and $\Delta S^{\ddagger} = -4(2)$ cal/(mol K), while using only the ^1H NMR data gives $\Delta H^{\ddagger} = 7.4(3)$ kcal/mol and $\Delta S^{\ddagger} = -6(2)$ cal/molK.

(23) Orpen, A. G. *J. Chem. Soc., Dalton Trans.* **1980**, 2509.

(24) (a) Masuda, H.; Taga, T.; Osaki, K.; Sugimoto, H.; Mori, M. *Bull. Chem. Soc. Jpn.* **1984**, *57*, 2345. (b) Hinckley, C. C.; Ali, I. A.; Robinson, P. D. *Acta Crystallogr., Sect. C: (Cryst. Struct. Commun.)* **1990**, *46*, 697. (c) Cheng, W.-K.; Wong, K.-Y.; Tong, W.-F.; Lai, T.-F.; Che, C.-M. *J. Chem. Soc., Dalton Trans.* **1992**, 91. (d) Che, C.-M.; Huang, J.-S.; Li, Z.-Y.; Poon, C.-K.; Tong, W.-F.; Lai, T.-F.; Cheng, M.-C.; Wang, C.-C.; Wang, Y. *Inorg. Chem.* **1992**, *31*, 5220.

(25) Crabtree, R. H.; Hlatky, G. G.; Holt, E. M. *J. Am. Chem. Soc.* **1983**, *105*, 7302.

(26) Smith, K.-T.; Tilset, M.; Kuhlman, R.; Caulton, K. G. *J. Am. Chem. Soc.* **1995**, *117*, 9473.

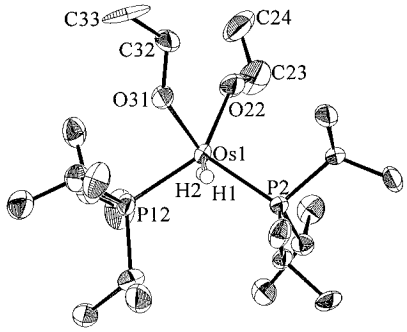

Figure 8. ORTEP drawing of $L_2OsH_2(OCH_2CF_3)_2$.

Table 4. Selected Bond Distances and Angles in $(P^iPr_3)_2OsH_2(OCH_2CF_3)_2$

	Distance (Å)		
Os1−P2	2.291(2)	Os1−O31	2.008(6)
Os1−P12	2.269(2)	O22−C23	1.41(2)
Os1−O22	2.017(7)	O31−C32	1.40(1)
	Angle (deg)		
P2−Os1−P12	112.50(8)	P12−Os1−O31	88.2(2)
P2−Os1−O22	99.1(2)	O22−Os1−O31	81.0(3)
P2−Os1−O31	142.5(3)	Os1−O22−C23	130.7(8)
P12−Os1−O22	139.4(2)	Os1−O31−C32	126.0(8)

phosphine. Triflate displaces methyl iodide, giving L_2OsH_2I-(OTf). After one more iteration of this process, complex **9** is formed.

Synthesis of $(P^iPr_3)_2OsH_2(OR_f)_2$. The bis-alkoxides with R_f = $CH(CF_3)_2$, (**12**) and CH_2CF_3, (**13**) are prepared by metathesis of two chlorides using $TlOR_f$. Unlike the dihalide compounds, **12** and **13** are quite soluble in arenes and are quite air sensitive, even as solids. Complex **12** can be stored indefinitely under argon, but solid **13** decomposes after several days at 25 °C, even under argon.

Structure of $(P^iPr_3)_2OsH_2(OCH_2CF_3)_2$. Alkoxides have one lone pair energetically higher than the other, so the position of the R group gives some insight into the nature of π-bonding. We therefore determined the structure of **13** via X-ray diffraction. Crystals were grown by dissolving the complex in a mixture of toluene and pentane and cooling at −20 °C overnight. The hydride ligands were not located crystallographically; they were placed in idealized positions using the program XHYDEX.[23] No positions of reasonable energy were found other than the two displayed in the ORTEP diagram (Figure 8). Selected bond distances and angles are given in Table 4. The $(P^iPr_3)_2OsH_2$ substructure of **13** is almost identical to that of **1**. The P−Os−P angle is 112.50(8)˚, with the HOsH plane perpendicular to it. The O−Os−O plane approximately bisects the P−Os−P and H−Os−H planes, with intersection angles of 48.3° and 43°, respectively (Figure 8). The Os−O22 and Os−O31 bond lengths (2.017(7) and 2.008(6) Å, respectively) are similar to others observed for Os(IV)−alkoxide bonds, which range from 1.909(4) to 2.2007(7) Å (seven distances average 1.98 Å).[24]

The Os−O−C angles are only slightly larger than expected for sp^2 hybridized oxygen (Os1−O22−C23 130.7(8)°, Os1−O31−C32 126.0(8)°). Atoms Os1, O22, and O31 are approximately coplanar with C23 and C32; distances from the O22−Os1−O31 plane to atoms C32 and C23 are only 0.03 and 0.43 Å, respectively (see Figure 9). One R group (with C32) points toward O22, while the other R group (with C23) points away from O31. Steric interactions with the phosphines discourage the placement of both alkoxide R groups pointing away from one another, while steric interactions of the alkoxide ligands with one another prevent them from pointing toward each other. The R group containing C23 is most likely forced

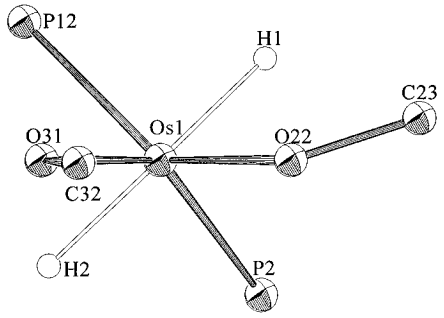

Figure 9. ORTEP diagram of $L_2OsH_2(OCH_2CF_3)_2$ emphasizing the near-coplanarity of Os1, O22, O31, C23, and C32. Alkyl groups on phosphines and CF_3 groups are not shown, for clarity.

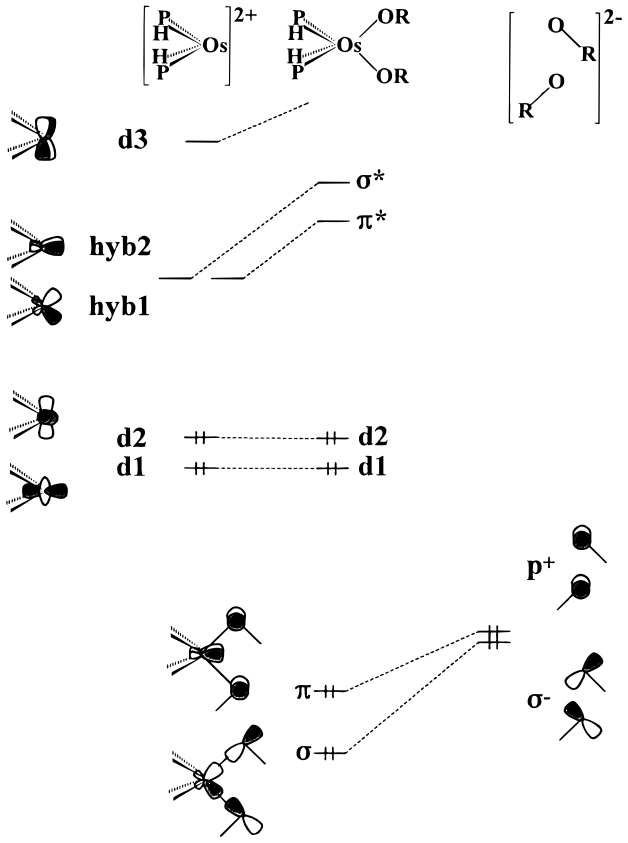

Figure 10. Interaction diagram for $[L_2Os(H)_2]^{2+}$ with $[(OR)_2]^{2-}$, showing the origin of the coplanarity of the C−O−Os−O−C atoms.

0.43 Å out of the O22−Os−O31 plane by steric interactions with a phosphine ligand. The near-planarity of Os, O22, O31, C23, and C32 results from conjugation of the two p_π orbitals on O22 and O31 with a d orbital on Os.

An interaction diagram for two alkoxides with the $(PR_3)_2H_2$-Os fragment is shown in Figure 10. This diagram is very similar in appearance to that for $L_2OsH_2Cl_2$,[14] except that the $(PR_3)_2H_2$ molecular fragment has been rotated by 45° to more clearly illustrate the interactions with the two alkoxide ligands in the observed structure. In Figure 10, hyb1 and hyb2 are degenerate in energy. Orbital hyb1 interacts with the σ^- combination of the alkoxide ligands to form σ-bonds, while hyb2 interacts with the nonhybridized oxygen lone pairs (p^+) to form a three-center, four-electron π-bonding interaction. This π-bonding interaction holds the carbon atoms α to oxygen coplanar with the OsO_2 plane.

Spectroscopic Characterization of $L_2OsH_2(OR)_2$. As well as "labeling" the lone pairs on oxygen in the X-ray structure, the R groups of the alkoxides label the π-donating groups for ^{19}F NMR investigations. No ^{19}F decoalescence is observed in

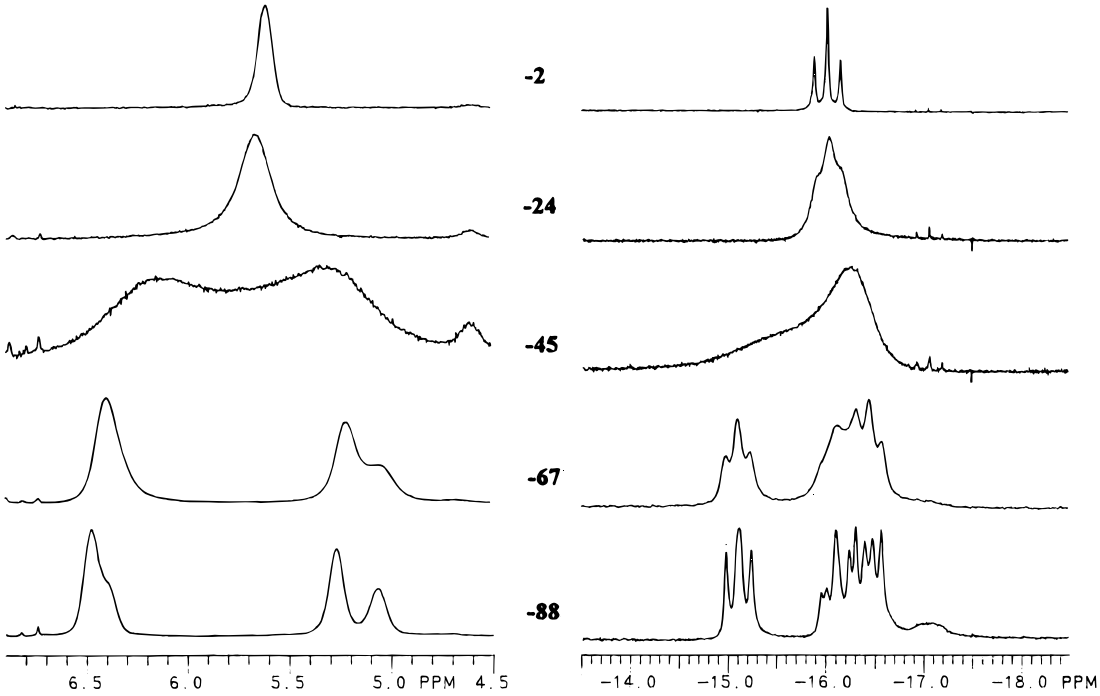

Figure 11. Methine region (left) and hydride region (right) ^{1}H NMR of $L_2OsH_2[OCH(CF_3)_2]_2$ in d_8-toluene at 300 MHz. Temperatures are given in °C.

13 at −90 °C in d_8-toluene. While two isomers were observed at low temperature for the halide complexes, the increased steric bulk of the alkoxide ligands could explain the observation of only one isomer for **13**. Furthermore, this complex must contain a C_2 axis or a molecular plane of symmetry (real or time-averaged) in solution. In the X-ray structure, no molecular symmetry is present, but a C_2 axis is destroyed only by the directionality of the alkoxide R groups. In solution, either the structure is different than it is in the solid state or (more likely) there is fast rotation around Os−O bonds at all available temperatures.

Hexafluoroisopropoxide **12** was investigated by variable-temperature ^{1}H and ^{19}F NMR. In observations on either nucleus, decoalescence was observed to several different signals. In this case, rotation around Os−O bonds is probably slowed, leading to several different rotamers. At least five ^{19}F signals, four methyne hydrogens, and four hydride signals are observed at −80 °C. These variable-temperature spectra are shown in Figures 11 (^{1}H) and 12 (^{19}F). The most likely explanation for the decoalescence is reduced molecular symmetry of **12** due to slowed rotation around Os−O, O−C, Os−P, and/or P−C bonds in this highly congested molecule.

Protonation of $(P^iPr_3)_2OsH_2(OR_f)_2$. Since the complex with R = CH_2CF_3 (**13**) is unstable, protonation reactions were more conveniently carried out on $L_2OsH_2[OCH(CF_3)_2]_2$ (**12**). Reaction of **12** with 1 equiv of HBF_4 at room temperature in CD_2Cl_2 causes a color change from red to a clear yellow solution. By NMR, the reaction yields a single hydride- and phosphorus-containing product. A doublet of doublets in the methyl region of ^{1}H NMR once again indicates cisoid phosphines. This species is characterized by a quartet of triplets in the hydride region of ^{1}H NMR, a quartet in ^{31}P{^{1}H} NMR, and a 13-line pattern in ^{19}F NMR. The hydride signal at −19.57 ppm shows coupling to two phosphorus (J_{HP} = 36.9 Hz) and three fluorine (J_{HF} = 20.5 Hz) nuclei. The ^{31}P signal (32.4 ppm) is also split by coupling to three ^{19}F nuclei (J_{PF} = 34.7 Hz). The selectively proton-coupled ^{31}P NMR spectrum shows a six-line pattern, due to additional coupling to two ^{1}H nuclei, with $J_{PH} \approx J_{PF}$. The outer-line separation of 177.1 Hz allows the calculation of J_{PH} = 36.5 Hz, in good agreement to that measured in ^{1}H NMR.

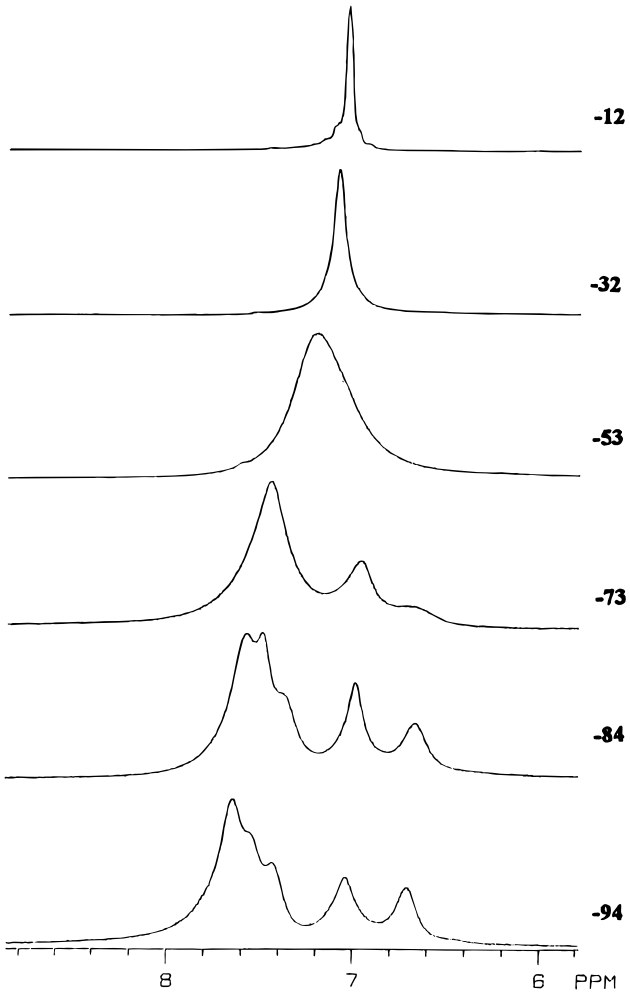

Figure 12. Variable-temperature ^{19}F NMR spectra of $L_2OsH_2[OCH(CF_3)_2]_2$ in d_8-toluene. Temperatures are given in °C.

The 13-line pattern of the fluorine signal (−242.27 ppm) is analyzed in terms of the known values, J_{HF} = 20.5 Hz and J_{PF} = 34.7 Hz. The outer-line separation of 219.0 Hz indicates

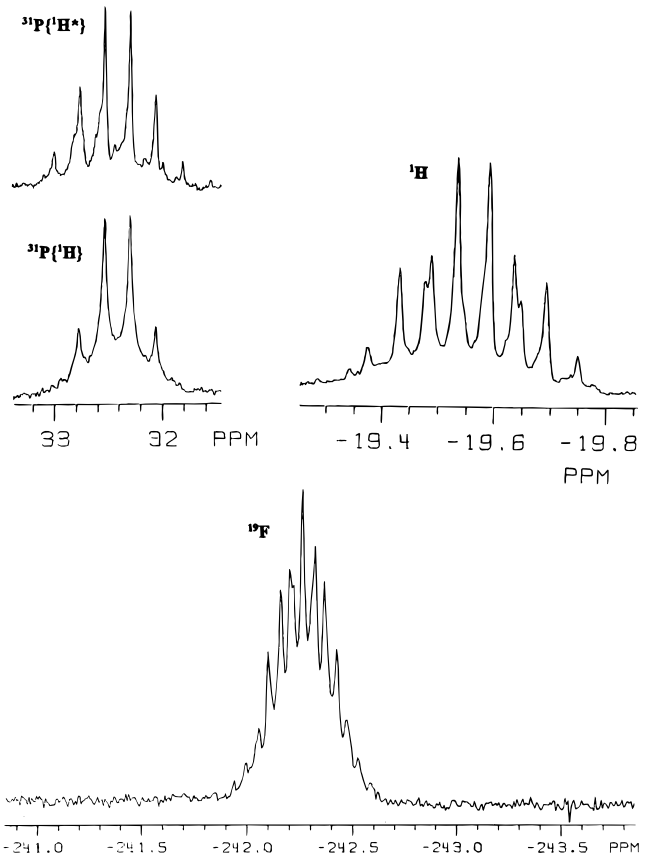

Figure 13. Spectral characterization of $[\{L_2OsH_2\}_2(\mu\text{-}F)_3]^+$: (upper left) fully ^{1}H-decoupled (^{31}P{^{1}H}) and selectively hydride-coupled (^{31}P-{^{1}H*} ^{31}P NMR; (upper right) ^{1}H NMR (hydride region, 360 MHz); (bottom) selected ^{19}F NMR.

coupling to *four* ^{31}P and *four* ^{1}H nuclei (calculated 220.8-Hz separation of outer lines). Since $J_{PF} \approx 2J_{HF}$ (within the resolution of the instrument), only 13 of the expected 25 lines of this quintet of quintets are observed. Thus, with the benefit of *three* $I = {}^1/_2$ nuclei, we are able to assign the structure completely by NMR to be $[\{L_2OsH_2\}_2(\mu\text{-}F)_3]^+$ (**14**), analogous to species **4** and **5** (eq 7). Figure 13 shows these NMR spectra. A somewhat related species, $[L_3Mo(H)_2]_2(\mu\text{-}F)_3^+$, has been reported.[25]

$$L_2OsH_2(OR)_2 + HBF_4 \rightarrow \underset{\mathbf{14}}{[L_2OsH_2]_2(\mu\text{-}F)_3^+} + ROH + ... \quad (7)$$

While the structure of **14** is conventional, its formation is remarkable. There are two potential sources of fluoride in the experiment: CF_3 groups and BF_4^-. There are several other ways to form **14**, although the reactions do not go as cleanly. Product **14** has been observed (by ^{1}H and ^{31}P NMR) as *one* product in each of the following reactions:

$$L_2OsH_2(OCH_2CF_3)_2 \rightarrow [\{L_2OsH_2\}_2(\mu\text{-}F)_3\}^+ + ... \quad (8)$$

$$L_2OsH_2Cl_2 + AgBF_4 \rightarrow [\{L_2OsH_2\}_2(\mu\text{-}F)_3]^+ + ... \quad (9)$$

$$L_2OsH_2Cl_2 + 2Me_4NF \rightarrow [\{L_2OsH_2\}_2(\mu\text{-}F)_3]^+ + ... \quad (10)$$

The reaction in eq 8 is the decomposition of **13** over a period of several days at ambient temperature in the solid state. In fact, **14** is by far the major hydride-containing component of this decomposition, and also a major product observed by ^{31}P NMR. In this reaction, the bridging fluorides clearly must come from CF_3 groups. Reaction 9 was mentioned earlier as one of few electrophilic additions to **1** which does *not* form **4**. In this case, the source of fluoride must be BF_4^-. The source of F^- in reaction 10, an attempted synthesis of $L_2OsH_2F_2$, is quite clear. In this reaction, **14** is only a minor component of the products.

In a reaction of **12** and 1.0 equiv of HBF_4 in an NMR tube, ^{19}F NMR revealed signals at −77.63, −77.77, and −78.05 (the CF_3 region), −153.51 (BF_4^- region), and −242.23 (μ-F). Since no signals were observed for CF_2 or CF groups, it seems likely that the fluorides are provided by the BF_4- anion rather than C−F moieties in this reaction. From this NMR tube, the volatile components were vacuum-transferred to another NMR tube. This colorless solution contained ether (from HBF_4/ether solution) and $(CF_3)_2CHOH$ as the only components. The nonvolatile components included a broad resonance at 3.8 ppm in ^{1}H NMR which could be from an anion like $BF_x[OCH(CF_3)_2]_{4-x}^-$. A trace of $P^iPr_3H^+$ was also observed.

Protonation of Another d^4 Six-Coordinate Hydride−Halide Complex: $(P^iPr_3)_2OsH_3Cl$. Noting that formation of trihalide-bridged dimers requires *two* halides/Os, we were interested in the protonation of other similar *hydride−monohalide* complexes. Reaction of L_2OsH_3Cl with excess HBF_4 in CD_2Cl_2 occurs very quickly even at −80 °C. The two major products of the reaction are $L_2OsH_7^+$ [26] and **4** (eq 11), identified by ^{1}H, ^{31}P chemical shifts, T_1 values, and decoalescence behavior. These two products are observed in an approximately 1:1 ratio. There are two other minor unidentified hydride-containing products. No intermediates are observed, even when the reaction is carefully monitored starting at −80 °C. A *possible* reaction pathway is shown in Scheme 2, based on experience with protonation reactions of the dihalide complexes. However, since *both* transfer of HCl and of H_2 are required to complete eq 11,

$$3L_2OsH_3Cl + 2H^+ \rightarrow \underset{\mathbf{4}}{[(L_2OsH_2)_2Cl_3]^+} + L_2Os(H)_3(H_2)_2^+ \quad (11)$$

the initial site of protonation (H or Cl) remains unknown. The better steric accessiblity of the halide (relative to hydride) makes them an attractive site for an electrophile.

Scheme 2

$$2L_2OsH_3Cl + H^+ \rightarrow [\{L_2OsH_2\}_2(\mu\text{-}Cl)(\mu\text{-}H)_2]^+ + HCl$$

$$L_2OsH_3Cl + HCl \rightarrow L_2OsH_4Cl_2$$

$$L_2OsH_4Cl_2 \rightarrow L_2OsH_2Cl_2 + H_2$$

$$L_2OsH_2Cl_2 + [\{L_2OsH_2\}_2(\mu\text{-}Cl)(\mu\text{-}H)_2]^+ \rightarrow [\{L_2OsH_2\}_2(\mu\text{-}Cl)_3]^+ + L_2OsH_4$$

$$L_2OsH_4 + H_2 \rightarrow L_2OsH_6$$

$$L_2OsH_6 + H^+ \rightarrow [L_2OsH_7]^+$$

Conclusions

With the possible exception of X = I, $L_2OsH_2X_2$ is protonated (or otherwise electrophilically attacked) at the X-ligand, rather than hydride. In fact, the L_2OsH_2 parts of these complexes very seldom take any part in the reactions at all. The remarkable difference in reactivity of iodide underscores how easily the site of protonation can be diverted from halide to hydride. A survey of available structural data shows that ∠M−(μ_2-X)−M becomes more acute for the heavier halides X. For iodide, this

Table 5. Crystallographic Data for$[(P^iPr_3)_2OsH_2(OSO_2CF_3)_2][(P^iPr_3)_2OsH_2(OSO_2CF_3)_2H_2O]$

formula[a]	$C_{40}H_{90}O_{13}P_4S_4F_{12}Os_2$	fw (g mol^{-1})	1639.66
a (Å)	19.916(3)	space group	$P\bar{1}$
b (Å)	20.260(4)	*T* (°C)	−172
c (Å)	19.824(3)	λ (Å)[a]	0.71069
α (deg)	115.54(1)	ρ_{calc} (g cm^{-3})	1.759
β (deg)	115.03(1)	μ (cm^{-1})	44.2
γ (deg)	63.57(1)°	$R(F_o)$[b]	0.0632
V (deg)	6192.85	$R_w(F_o)$[c]	0.0623
Z (deg)	4		

[a] Graphite monochromator. [b] $R = \sum||F_o| - |F_c||/\sum|F_o|$. [c] $R_w = [\sum w(|F_o| - |F_c|)^2/\sum w|F_o|^2]^{1/2}$ where $w = 1/\sigma^2(|F_o|)$.

angle is in the range 55−87°.[27] This would aggravate X/P^{i}Pr$_3$ and P^{i}Pr$_3$/P^{i}Pr$_3$ steric repulsions in $(L_2OsH_2)_2(\mu\text{-}I)_3^+$, and may explain why the iodo derivative shows consistently different behavior when $OsH_2X_2L_2$ undergoes electrophilic attack.

Electrophilic removal of halide ligands provides access to one hemisphere of these osmium complexes. When X = Br or Cl, the "open face" can be filled by forming halide bridges, but this reaction pattern is not observed when X = I. Instead, even the weakly-coordinating triflate ligand can bind to this highly reactive center. In addition, protonolysis has led to activation of B−F, and even C−F bonds.

Unlike H^+, other electrophiles seem to uniformly attack at halide in preference to hydride. Steric factors may once again be an important influence, when the electrophile itself has significant steric bulk. The electron density of a hydride ligand resides primarily in the *metal−hydride bond*, which is generally less accessible than *lone pairs* on a halide ligand. Bulkier electrophiles may not be able to gain access to the M−H bonds.

Experimental Section

All reactions and manipulations were conducted using standard Schlenk and glovebox techniques. Solvents were dried and distilled under nitrogen or argon and stored in air-tight solvent bulbs with Teflon closures. All NMR solvents were dried, vacuum-transferred, and stored in a glovebox. Complexes $(P^iPr_3)_2OsH_2X_2$ (X = Cl, Br, I)[14] and $[L_2OsH_2](Cl)_3^+$ [4] were synthesized according to published procedures. Proton NMR spectra were obtained on a Varian XL-300, a Nicolet 360 MHz, or a Bruker AM 500 spectrometer, while ^{31}P and ^{19}F spectra were recorded on a Nicolet 360 MHz instrument. All T_1 measurements were made at 300 MHz using the inversion−recovery method. Chemical shifts are referenced to residual protio solvent peaks (^{1}H), external H_3PO_4 (^{31}P), or external $CFCl_3$ (^{19}F). Temperatures were standardized according to the peak separation of CH_3OH; temperatures below −100 °C require extrapolation and may be less reliable. Infrared spectra were recorded on a Nicolet 510P FT-IR spectrometer. The mixture of $CDFCl_2/CDF_2Cl$ was synthesized by the method of Siegel,[28] and stored at −20 °C in a glass bulb with Teflon closure. Elemental analyses were performed by Desert Analytics, Tucson, AZ.

Synthesis of $[\{(P^iPr_3)_2H_2Os\}_2(\mu\text{-}Br)_3]BF_4$ (5). In a Schlenk flask, $L_2OsH_2Br_2$ (0.170 g, 0.253 mmol) was dissolved in CH_2Cl_2 (10 mL). Via syringe, 400 μL of HBF_4 (54% in ether, 2.9 mmol) was added. The solution slowly changed in color to pale yellow, as the solution was stirred for 1 h. The solvent was then removed in vacuo, and the product washed with ether (5 × 10 mL). Yield = 0.120 g (0.089 mmol, 70%). ^{1}H NMR (CD_2Cl_2, 20 °C): 2.39 (mult, 6H), 1.32 (dd, J_{HP} = 15.0 Hz, J_{HH} = 7.5 Hz), −15.19 (t, J_{HP} = 33.2 Hz). T_1 of signal at −15.l9 (−77 °C, 300 MHz) = 200(4) ms. ^{31}P{^{1}H} NMR (CD_2Cl_2, 20 °C): 22.4 (s). IR(KBr): ν_{OsH} = 2199, 2167 cm^{-1}. Anal. Calcd: C, 31.98; H, 6.56, Found: C, 31.78%; H, 6.47.

Reaction of 4 with ^{13}CO. Complex **4** (10 mg) was dissolved in CD_2Cl_2 in an NMR tube fitted with a Teflon closure. After 3 freeze−pump−thaw cycles, ^{13}CO was introduced into the tube. The tube was shaken and ^{31}P, ^{1}H, and ^{13}C NMR spectra were recorded. Spectra were recorded after four further additions of ^{13}CO, after which all signals for complex **4** had disappeared. An intermediate was observed with ^{31}P signal at 20.4 ppm. The final products were $(P^iPr_3)_2OsCl(^{13}CO)_3^+$ and $(P^iPr_3)_2OsCl_2(^{13}CO)_2$. The identity of $L_2OsCl_2(^{13}CO)_2$ was confirmed by independent preparation from **1** and ^{13}CO in CD_2Cl_2.

$(P^iPr_3)_2OsCl_2(^{13}CO)_2$ (6). ^{1}H NMR (CD_2Cl_2): 2.96 (mult, 6H), 1.40 (apparent q, 36H). Selected ^{13}C NMR (CD_2Cl_2): 176.90 (t, $^2J_{CP}$ = 7.9 Hz). ^{31}P{^{1}H} (CD_2Cl_2): 8.1 (s).

$(P^iPr_3)_2OsCl(^{13}CO)_3^+$ (7). ^{1}H NMR (CD_2Cl_2): 2.89 (mult, 6H), 1.45 (apparent q, 36H). selected ^{13}C NMR (CD_2Cl_2): 176.60 (td, $^2J_{CP}$ = 8.0 Hz, $^2J_{CC}$ = 3.9 Hz), 168.61 (tt, $^2J_{CP}$ = 6.1 Hz, $^2J_{CC}$ = 3.9 Hz). ^{31}P{^{1}H} (CD_2Cl_2): 17.3 (s).

$[(P^iPr_3)_2OsH_3I_2]^+$ (8). An extended NMR tube was charged with a solution of **3** (0.012 g, 0.019 mmol) in CD_2Cl_2 (0.15 mL). In a Schlenk flask, one small drop of HOTf (approximately 10 equiv) was dissolved in 0.3 mL of CD_2Cl_2. The tube was attached to a Schlenk line via a vacuum adaptor and cooled in liquid nitrogen. The acid solution was then added to the osmium solution via cannula transfer. The tube was subjected to 3 freeze-pump−thaw−degas cycles (warming in a −80 °C cold bath to degas) and flame-sealed under vacuum. The NMR probe was pre-cooled to −70 °C. ^{1}H NMR (CD_2Cl_2): at −70 °C, 2.16 (br, 6H), 1.28 (dd, J = 16.2, 6.0 Hz, 36H), −7.31 (br, 2H); at −28.2 °C, −7.04 (t, J_{HP} = 14.0 Hz). T_1 measurements (300 MHz): −68/33, −77/32, −88/35 °C/ms. ^{31}P{^{1}H} NMR (CD_2Cl_2, −70 °C): 99.4 (s). The final product observed was **$P^iPr_3H^+$**. ^{1}H (CD_2Cl_2, 20 °C): 6.03 (dq, J_{HP} = 472 Hz, J_{HH} = 4.3 Hz, 1H), 2.75 (mult, 3H), 1.54 (dd, *J* = 17.7, 7.2 Hz, 36H). The HP coupling constant and chemical shift of the PH resonance vary slightly with acid concentration.

Synthesis of $L_2OsH_2(OSO_2CF_3)_2$ (9). Complex **1** (0.232 g, 0.303 mmol) was dissolved in CH_2Cl_2 (10 mL). Via cannula, a solution of $MeOT_f$ (0.482 g, 2.94 mmol) in CH_2Cl_2 (5 mL) was added. The solution was stirred for 8 h, and the volatiles were removed in vacuo. Yield = 0.201 g (0.248 mmol, 82%). Compound **9** is extremely hygroscopic, and even this product contains some H_2O (ca. 4% according to integration in ^{1}H NMR). Cocrystals (1:1) of **9** and **10** were grown over a period of 10 days from CH_2Cl_2 and ether. ^{1}H NMR (CD_2Cl_2, 20 °C): 2.37 (mult, 6H), 1.35 (dd, *J* = 13.8, 7.0 Hz), −17.25 (t, J_{HP} = 35.3 Hz). ^{31}P{^{1}H} NMR (CD_2Cl_2, 20 °C): 49.1 (s). Anal. Calcd: C, 29.63; H, 5.47. Found C, 27.90; H, 5.33.

X-ray Diffraction Study of $[L_2OsH_2(OSO_2CF_3)_2][L_2OsH_2(OSO_2CF_3)_2(H_2O)]$. A small well-formed crystal was cleaved from a larger sample and affixed to the end of a glass fiber using silicone grease, and the mounted sample was then transferred to the goniostat where it was cooled to −172 °C for characterization and data collection. Standard inert atmosphere handling techniques were used throughout the investigation. A systematic search of a limited hemisphere of reciprocal space located a set of data with no symmetry or systematic absences, indicating a triclinic space group (Table 5). Subsequent solution and refinement of the structure confirmed the centrosymmetric $P\bar{1}$ to be the proper space group. Data were collected ($6° < 2\theta < 45°$) using a standard moving-crystal moving-detector technique with fixed background counts at each extreme of the scan. Data were corrected for Lorentz and polarization terms and equivalent data averaged. The structure was solved by direct methods (SHELXS-86) and Fourier techniques. Four independent molecules are present in the cell. The data were not of sufficient quality to locate the hydrogen atoms in the molecules, so it is not possible to determine either the presence or number of hydrides present or to verify the identity of the coordinated water on two of the molecules. No attempt was made to include hydrogen atoms in the refinement. A final difference Fourier was essentially featureless, the largest peaks (up to 2.1 e/Å^3) lying at the site of the metal atom. The results of the structure determination are shown in Tables 1, 2, 5, and 6 and Figures 3 and 4.

$(P^iPr_3)_2OsH_2(OSO_2CF_3)_2(H_2O)$ (10). Synthesis of this complex in pure form is nearly impossible due to the additional reactions of **9** with H_2O. ^{1}H NMR (freons): at −13 °C), 2.19 (mult, CH, 6H), 1.20 (dd, *J* = 14.7, 6.0 Hz), −17.63 (t, J_{HP} = 33.8 Hz); at −108 °C, −16.38

(27) (a) Barbati, A.; Calderazzo, F.; Poli, R.; Zanazzi, P. F. *J. Chem. Soc., Dalton Trans.* **1986**, 2569. (b) Cotton, F. A.; Poli, R. *Inorg. Chem.* **1987**, *26*, 3310. (c) Calderazzo, F.; Marchetti, F.; Poli, R.; Vitali, D. *J. Chem. Soc., Dalton Trans.* **1982**, 1665. (d) Bowmaker, G. A.; Camus, A.; Healy, P. C.; Skelton, B. W.; White, A. H. *Inorg. Chem.* **1989**, *28*, 3883. (e) Morse, D. B.; Rauchfuss, T. B.; Wilson, S. R. *J. Am. Chem. Soc.* **1990**, *112*, 1860. (f) Gordon, J. C.; Mui, H. D.; Poli, R.; Ahmed, K. J. *Polyhedron* **1991**, *10*, 1667. (g) Nolte, M. J.; Singleton, E.; van der Stok, E. *Acta Crystallogr., Sect. B* **1978**, *34*, 1684. (h) Calderazzo, F.; Gingl, F.; Pampaloni, G.; Rocchi, L.; Strahle, J. *Chem. Ber.* **1992**, *125*, 1005.

(28) Siegel, J. S.; Anet, F. A. L. *J. Org. Chem.* **1988**, *53*, 2629.

Table 6. Fractional Coordinates and Isotropic Thermal Parameters[a]

	10^4x	10^4y	10^4z	$10B_{iso}$		10^4x	10^4y	10^4z	$10B_{iso}$
Os(1)A	2958.1(4)	2783.6(4)	3142.1(4)	11	F(38)B	9280(7)	997(7)	582(6)	30
O(2)A	2958(7)	3983(7)	3500(7)	15	Os(1)C	12967.0(4)	2237.9(4)	7837.7(4)	13
P(3)A	4280(3)	2593(3)	3721(3)	13	P(2)C	12385(3)	3387(3)	7584(3)	13
C(4)A	4565(9)	2935(11)	4822(10)	11	C(3)C	12998(10)	3825(12)	7538(11)	25
C(5)A	4282(11)	2533(12)	5134(11)	23	C(4)C	13576(12)	4083(13)	8351(11)	25
C(6)A	4247(11)	3813(13)	5177(11)	23	C(5)C	13472(12)	3297(12)	6932(12)	23
C(7)A	4917(11)	1579(12)	3472(11)	20	C(6)C	11658(11)	3206(12)	6591(12)	22
C(8)A	5086(10)	1283(12)	2677(12)	22	C(7)C	12027(11)	2510(11)	5963(10)	17
C(9)A	5737(12)	1360(14)	4119(13)	34	C(8)C	11184(12)	3930(12)	6310(12)	23
C(10)A	4608(10)	3165(11)	3505(10)	15	C(9)C	11824(11)	4177(11)	8256(11)	18
C(11)A	4400(11)	3117(13)	2635(12)	23	C(10)C	11066(11)	4042(12)	8138(12)	21
C(12)A	5508(11)	3082(14)	3903(12)	26	C(11)C	11638(12)	5018(12)	8285(14)	30
P(13)A	2669(3)	1633(3)	2537(3)	14	P(12)C	13514(3)	2364(3)	9130(3)	19
C(14)A	2711(11)	1151(12)	3164(11)	17	C(13)C	14158(14)	2995(14)	9708(12)	34
C(15)A	3579(12)	780(12)	3622(12)	22	C(14)C	14944(12)	2598(14)	9420(13)	30
C(16)A	2245(13)	1672(14)	3751(14)	35	C(15)C	14356(15)	3225(16)	10619(12)	45
C(17)A	3297(11)	885(12)	1918(10)	20	C(16)C	14139(12)	1363(15)	9060(14)	34
C(18)A	3301(12)	32(14)	1658(12)	29	C(17)C	13724(11)	762(12)	8405(13)	29
C(19)A	3158(11)	1086(12)	1196(11)	20	C(18)C	14481(13)	1195(15)	9889(13)	39
C(20)A	1653(10)	1808(12)	1875(10)	23	C(19)C	12905(13)	2650(12)	9769(12)	25
C(21)A	996(10)	2389(12)	2283(11)	18	C(20)C	12409(13)	2097(14)	9459(12)	29
C(22)A	1422(12)	1056(13)	1346(12)	27	C(21)C	12390(14)	3518(14)	9901(13)	34
O(23)A	2153(7)	3350(7)	3914(7)	17	O(22)C	12262(7)	1533(8)	7007(7)	19
S(24)A	1958(3)	4057(3)	4530(3)	17	S(23)C	11480(3)	1506(3)	6882(3)	24
O(25)A	2217(8)	3975(9)	5289(8)	30	O(24)C	11361(9)	1566(11)	7567(9)	48
O(26)A	2088(8)	4690(8)	4497(8)	25	O(25)C	10849(8)	1978(9)	6411(10)	39
C(27)A	878(12)	4321(13)	4244(12)	25	C(26)C	11585(12)	542(14)	6303(13)	31
F(28)A	686(6)	3790(7)	4260(7)	31	F(27)C	12145(8)	48(9)	6681(10)	61
F(29)A	558(6)	4414(8)	3541(7)	33	F(28)C	11762(8)	383(8)	5660(8)	49
F(30)A	610(7)	4989(7)	4761(7)	31	F(29)C	10924(8)	371(9)	6073(9)	52
O(31)A	1863(7)	3337(7)	2393(7)	18	O(30)C	13627(7)	1391(8)	7030(7)	27
S(32)A	1743(3)	3620(3)	1758(3)	17	S(31)C	14429(3)	1039(3)	6982(3)	17
O(33)A	1553(8)	3114(8)	998(7)	25	O(32)C	14791(8)	315(8)	7127(8)	26
O(34)A	2313(7)	3976(8)	1947(7)	22	O(33)C	14862(8)	1550(9)	7332(8)	29
C(35)A	866(11)	4417(12)	1840(12)	23	C(34)C	14222(11)	804(12)	5918(12)	24
F(36)A	970(7)	4926(7)	2556(7)	38	F(35)C	13735(8)	405(8)	5537(7)	37
F(37)A	622(6)	4796(7)	1333(7)	29	F(36)C	13911(7)	1435(7)	5712(7)	33
F(38)A	273(6)	4199(8)	1741(8)	34	F(37)C	14869(7)	401(8)	5720(7)	40
Os(1)B	8163.0(4)	2064.7(4)	2836.2(4)	11	Os(1)D	7701.3(4)	2911.1(5)	8062.0(4)	13
O(2)B	8497(7)	873(7)	2862(7)	18	P(2)D	7434(3)	1783(3)	7527(3)	13
P(3)B	8745(3)	2259(3)	4160(3)	14	C(3)D	7408(10)	1358(11)	8186(10)	17
C(4)B	9863(11)	1870(14)	4441(12)	25	C(4)D	8223(11)	1078(13)	8712(12)	29
C(5)B	10172(11)	2239(16)	4118(11)	32	C(5)D	6822(11)	1907(11)	8650(11)	22
C(6)B	10161(11)	994(13)	4129(11)	23	C(6)D	6417(11)	2023(12)	6875(10)	20
C(7)B	8497(10)	3292(11)	4774(10)	16	C(7)D	5841(10)	2758(11)	7253(11)	21
C(8)B	7700(11)	3607(11)	4905(10)	18	C(8)D	6095(11)	1348(13)	6418(11)	27
C(9)B	9124(12)	3482(13)	5579(13)	28	C(9)D	8026(11)	971(12)	6919(11)	23
C(10)B	8516(11)	1692(11)	4515(11)	19	C(10)D	8027(10)	164(10)	6751(11)	19
C(11)B	8916(11)	1767(12)	5407(11)	24	C(11)D	7868(11)	1114(11)	6159(11)	22
C(12)B	7633(10)	1804(12)	4325(11)	18	P(12)D	9000(3)	2747(3)	8614(3)	16
P(13)B	7587(3)	3211(3)	2513(3)	12	C(13)D	9608(9)	2423(11)	7965(11)	20
C(14)B	6932(11)	3032(12)	1490(12)	22	C(14)D	9363(11)	2958(14)	7483(11)	30
C(15)B	6427(12)	3787(13)	1235(12)	24	C(15)D	9677(11)	1568(13)	7452(12)	29
C(16)B	7336(12)	2423(12)	855(12)	25	C(16)D	9564(11)	2123(12)	9257(11)	25
C(17)B	6942(11)	3996(12)	3106(12)	23	C(17)D	9350(12)	2504(14)	10039(11)	31
C(18)B	6703(12)	4829(11)	3097(12)	23	C(18)D	10481(11)	1816(16)	9429(14)	41
C(19)B	6196(11)	3822(13)	2951(13)	26	C(19)D	8965(12)	3740(13)	9210(12)	32
C(20)B	8237(11)	3663(12)	2536(12)	22	C(20)D	8369(12)	4340(13)	8792(13)	31
C(21)B	8686(12)	4018(12)	3397(12)	24	C(21)D	9792(13)	3845(13)	9564(12)	33
C(22)B	8828(11)	3115(13)	2076(12)	26	O(22)D	6918(6)	3623(7)	7324(7)	18
O(23)B	7365(7)	1548(8)	1777(7)	21	S(23)D	6795(3)	3538(3)	6501(3)	22
S(24)B	6740(3)	1296(3)	1684(3)	20	O(24)D	6255(10)	3153(10)	5948(9)	46
O(25)B	5980(8)	1831(9)	1524(9)	35	O(25)D	7492(9)	3299(12)	6315(10)	58
O(26)B	6945(8)	923(9)	2249(8)	35	C(26)D	6326(14)	4513(14)	6511(12)	36
C(27)B	6796(12)	525(13)	795(13)	27	F(27)D	6728(13)	4959(10)	7021(10)	97
F(28)B	6643(9)	777(9)	211(7)	50	F(28)D	5645(10)	4810(9)	6686(9)	68
F(29)B	6283(7)	166(8)	567(7)	36	F(29)D	6149(9)	4588(9)	5805(8)	57
F(30)B	7500(7)	3(8)	865(8)	46	O(30)D	6961(7)	3852(7)	8728(7)	23
O(31)B	8931(7)	1422(8)	2024(7)	21	S(31)D	6940(3)	4231(3)	9555(3)	20
S(32)B	9545(3)	706(3)	1851(3)	21	O(32)D	7318(7)	3705(8)	10014(7)	27
O(33)B	10291(8)	778(10)	2101(8)	37	O(33)D	7104(8)	4934(9)	9876(8)	24
O(34)B	9504(9)	85(8)	1991(8)	30	C(34)D	5916(11)	4480(12)	9423(12)	25
C(35)B	9273(12)	451(12)	780(11)	19	F(35)D	5724(7)	4934(8)	10079(7)	49
F(36)B	8565(7)	390(8)	461(7)	38	F(36)D	5668(7)	3886(8)	9147(7)	38
F(37)B	9790(7)	−214(7)	517(7)	35	F(37)D	5482(7)	4897(9)	8908(9)	52

[a] Isotropic values for those atoms refined anisotropically are calculated using the formual given by: Hamilton, W. C. *Acta Crystallogr.* **1959**, *12*, 609.

(dd, J_{HP} = 33.9 Hz, J_{HP} = 42.6 Hz), −18.70 (br t, J_{HP} = 30 Hz). $^{31}P\{^1H\}$ NMR (freons): at −30 °C), 29.9 (br s); at −105 °C, 14.0 (s), 46.4 (s).

$(P^iPr_3)_2OsH_2(OSO_2CF_3)I$ (11). Selected ^1H (CD_2Cl_2, 20 °C): −13.99 (t, J_{HP} = 31.5 Hz). ^{31}P (CD_2Cl_2, 20 °C): 16.0 (s).

Synthesis of $(P^iPr_3)_2OsH_2[OCH(CF_3)_2]_2$ (12). A Schlenk flask was charged with **1** (0.150 g, 0.257 mmol) and $TlOCH(CF_3)_2$ (0.192 g, 0.517 mmol). Via cannula, benzene (15 mL) was added. After the mixture was stirred for 5 min, the resulting red solution was filtered through a glass frit (to remove TlCl) and the solid washed with benzene (2 × 5 mL). Evaporation of the benzene yields a dark orange solid. Yield = 0.183 g (0.216 mmol, 84%). Anal. Calcd: C, 34.04; H, 5.48. Found: C, 32.97; H, 5.43. ^1H (d_8-toluene, 20 °C) 5.56 (sept, J_{HF} = 5.9, 2H), 1.19 (mult, 6H), 1.03 (dd, J_{HP} = 13.8 Hz, J = 7.5 Hz, 36H), −16.04 (t, J_{HP} = 39.6 Hz, 2H). $^{31}P\{^1H\}$ NMR (CD_2Cl_2, 20 °C): 37.1 (s). ^{19}F (d_8-toluene, 20 °C): −71.4 (s). IR (KBr): ν_{OsH} = 2175 (br).

Synthesis of $(P^iPr_3)_2OsH_2(OCH_2CF_3)_2$ (13). This compound was prepared as described for **12**, reacting $L_2OsH_2Cl_2$ (0.110 g, 0.189 mmol) with $TlOCH_2CF_3$ (0.115 g, 0.379 mmol). Yield = 0.071 g (0.100 mmol, 53%). Crystals were grown by dissolving impure **13** (0.100 g, from a different preparation) in toluene (1 mL) and pentane (10 mL) and storing in a −20 °C freezer for 16 h. Recrystallized yield = 41%. Even in the solid state under argon, this compound decomposes on the time scale of weeks. Anal. Calcd: C, 37.18; H, 6.81. Found: C, 37.38; H, 6.95. ^1H NMR (C_6D_6, 20 °C): 4.82 (q, J_{HF} = 9.8 Hz, 4H), 1.95 (mult, 6H), 1.01 (dd, J_{HP} = 13.5 Hz, J = 7.2 Hz, 36H), −15.55 (t, J = 39.8 Hz, 2H). $^{31}P\{^1H\}$ NMR (C_6D_6, 20 °C): 42.1 (s). ^{19}F NMR (d_8-toluene, 20 °C): −72.97 (t, J_{FH} = 9.8 Hz). IR (KBr): ν_{OsH} = 2190 (w), 2163 (sh), 2145 (s).

X-ray Diffraction Study of $(P^iPr_3)_2OsH_2(OCH_2CF_3)_2$. A crystal of suitable size was mounted in a nitrogen atmosphere glovebag using silicone grease. The crystal was then transferred to a goniostat where it was cooled to −175 °C for characterization and data collection. A preliminary search revealed a primitive monoclinic cell. Following complete intensity data collection, the conditions $l = 2n$ for $h0l$ and $k = 2n$ for $0k0$ uniquely determined space group $P2_1/c$. Four standards measured every 300 data showed no significant trends. The structure was solved by a combination of direct methods (SHELXS-86) and Fourier techniques. The position of the osmium atom was obtained from an initial E-map. The positions of the remaining non-hydrogen atoms were obtained from subsequent iterations of a least-squares refinement followed by a difference Fourier calculation. The data were corrected for absorption (transmission factors from 0.43 to 0.72). The fluorine atoms are disordered. A reasonably clean difference map was eventually obtained by modeling one of the CF_3 groups with six partial occupancy fluorine atoms and the other CF_3 group with seven partial occupancy fluorines. After refining the occupancies, they were normalized to give a total occupancy of 3 for each CF_3 group and they were then fixed to avoid correlation with the thermal parameters. Hydrogens bonded to carbon were included in fixed calculated positions with thermal parameters fixed at one plus the isotropic thermal parameter of the carbon to which it was bonded. The anticipated hydride ligands were not observed and were not included in any of the refinements; they were included in calculations such as the density, the absorption coefficient, and $F(000)$. In the final cycles of refinement, the ordered non-hydrogen atoms were varied with anisotropic thermal parameters, and the disordered fluorines were varied with isotropic parameters. The largest peak in the final difference map was an osmium residual of 1.8 and the deepest hole was 1.2 e/Å^3. The results of the structure determination are shown in Tables 4, 7, and 8 and in Figures 8 and 9.

$\{(P^iPr_3)_2OsH_2\}_2(\mu\text{-}F)_3^+$ (15). To an NMR tube containing a solution of $L_2OsH_2[OCH(CF_3)_2]_2$ (0.012 g, 0.014mmol) in CD_2Cl_2 was added HBF_4 (2.0 μL, 0.015 mmol). The reaction was complete within less than 10 min. ^1H (CD_2Cl_2, 20 °C): 2.16 (mult, 12H), 1.27 (dd, J = 6.3, 12.9 Hz, 72H), −19.57 (qt, J_{HF} = 20.5 Hz, J_{HP} = 36.9 Hz, 4H). T_1 of resonance at −15.97: −78/201, −68/171, −58/173 °C/ms. $^{31}P\{^1H\}$ (CD_2Cl_2, 20 °C): 32.4 (q, J_{PF} = 34.6 Hz). Selectively hydride-coupled ^{31}P: 32.4 (six-line pattern, J_{PF} = 34.6 Hz, J_{PH} = 36.5 Hz). ^{19}F (CD_2Cl_2, 20 °C): −242.23 (quint of quint, J_{FP} = 35.4 Hz, J_{FH} = 19.2 Hz).

Table 7. Crystallographic Data for $(P^iPr_3)_2OsH_2(OCH_2CF_3)_2$

formula[a]	$C_{22}H_{48}F_6O_2OsP_2$	fw (g mol^{-1})	710.76
a (Å)	8.831(2)	space group	$P2_1/c$
b (Å)	16.680(4)	T (°C)	−175
c (Å)	19.820(5)	λ (Å)[a]	0.71069
β (deg)	93.97(1)	ρ_{calc} =(g cm^{-1})	1.621
V (Å^3)	2912.38	μ (cm^{-1})	45.436
Z	4	$R(F_o)$[b]	0.0493
		$R_w(F_o)$[c]	0.0474

[a] Graphite monochromator. [b] $R = \sum||F_o| - |F_c||/\sum|F_o|$. [c] $R_w = [\sum w(|F_o| - |F_c|)^2/\sum w|F_o|^2]^{1/2}$ where $w = 1/\sigma^2(|F_o|)$.

Table 8. Fractional Coordinates and Isotropic Thermal Parameters[a] for $(P^iPr_3)_2OsH_2(OCH_2CF_3)_2$

OS(1)	2849.0(4)	7299.6(2)	3196.8(2)	21
P(2)	1955(2)	6457(1)	3992(1)	18
C(3)	3027(10)	6490(5)	4844(4)	22
C(4)	4711(11)	6258(6)	4809(5)	32
C(5)	2344(12)	6039(6)	5420(4)	32
C(6)	−38(10)	6467(6)	4232(4)	24
C(7)	−434(10)	7249(6)	4591(5)	33
C(8)	−1229(11)	6345(7)	3635(5)	36
C(9)	2124(10)	5435(5)	3627(4)	24
C(10)	1638(11)	4733(6)	4060(5)	31
C(11)	3684(13)	5252(6)	3361(5)	37
P(12)	3088(3)	8583(1)	3570(1)	22
C(13)	1738(12)	9224(6)	3010(5)	35
C(14)	77(13)	9018(8)	3094(7)	52
C(15)	2064(12)	9184(6)	2295(5)	36
C(16)	4934(12)	9007(7)	3360(5)	38
C(17)	5101(14)	9913(7)	3495(6)	45
C(18)	6344(12)	8579(7)	3698(6)	43
C(19)	2627(15)	8834(7)	4433(5)	44
C(20)	2131(13)	9683(6)	4598(6)	39
C(21)	4097(16)	8633(7)	4935(5)	50
O(22)	2130(9)	6694(5)	2354(3)	42
C(23)	656(18)	6495(10)	2094(6)	68
C(24)	461(19)	6558(9)	1363(7)	65
F(25)	869(29)	7159(15)	1098(12)	70(5)
F(26)	1495(33)	6363(22)	994(14)	73(6)
F(27)	1702(24)	6833(16)	985(10)	61(4)
F(28)	1307(17)	5840(10)	1228(8)	53(3)
F(29)	330(17)	7489(9)	1393(8)	56(3)
F(30)	−837(10)	6371(5)	1097(4)	42(2)
O(31)	4638(9)	7491(4)	2645(4)	44
C(32)	4813(22)	7196(8)	1995(8)	80
C(33)	6159(15)	7557(11)	1729(5)	62
F(34)	6514(14)	7448(8)	1148(6)	34(2)
F(35)	7269(15)	8001(8)	2041(6)	41(2)
F(36)	7027(26)	6770(16)	2104(11)	43(5)
F(37)	5266(17)	8375(9)	1590(7)	45(3)
F(38)	7305(22)	7183(14)	2132(10)	39(4)
F(39)	6456(23)	8217(12)	1744(9)	54(4)
F(40)	6247(15)	7111(9)	1076(7)	34(3)

[a] Isotropic values for those atoms refined anisotropically are calculated using the formula given by: Hamilton, W. C. *Acta Crystallogr.* **1959**, *12*, 609.

Acknowledgment. This work was supported by the National Science Foundation and by a fellowship from G. E. Plastics.

Supporting Information Available: Tables of crystallographic data and anisitropic thermal parameters (7 pages). See any current masthead page for ordering and Internet access instructions.

JA960369H